

Organic characterisation of cave drip water by LC-OCD and fluorescence analysis

Rutledge, Helen; Andersen, Martin S.; Baker, Andy; Chinu, Khorshed J.; Cuthbert, Mark O.; Jex, Catherine N.; Marjo, Christopher E.; Markowska, Monika; Rau, Gabriel C.

DOI:
[10.1016/j.gca.2015.05.042](https://doi.org/10.1016/j.gca.2015.05.042)

License:
Creative Commons: Attribution-NonCommercial-NoDerivs (CC BY-NC-ND)

Document Version
Peer reviewed version

Citation for published version (Harvard):
Rutledge, H, Andersen, MS, Baker, A, Chinu, KJ, Cuthbert, MO, Jex, CN, Marjo, CE, Markowska, M & Rau, GC 2015, 'Organic characterisation of cave drip water by LC-OCD and fluorescence analysis', *Geochimica et Cosmochimica Acta*, vol. 166, pp. 15-28. <https://doi.org/10.1016/j.gca.2015.05.042>

[Link to publication on Research at Birmingham portal](#)

Publisher Rights Statement:

After an embargo period, this document is subject to the terms of a Creative Commons Non-Commercial No Derivatives license.

Checked October 2015

General rights

Unless a licence is specified above, all rights (including copyright and moral rights) in this document are retained by the authors and/or the copyright holders. The express permission of the copyright holder must be obtained for any use of this material other than for purposes permitted by law.

- Users may freely distribute the URL that is used to identify this publication.
- Users may download and/or print one copy of the publication from the University of Birmingham research portal for the purpose of private study or non-commercial research.
- User may use extracts from the document in line with the concept of 'fair dealing' under the Copyright, Designs and Patents Act 1988 (?)
- Users may not further distribute the material nor use it for the purposes of commercial gain.

Where a licence is displayed above, please note the terms and conditions of the licence govern your use of this document.

When citing, please reference the published version.

Take down policy

While the University of Birmingham exercises care and attention in making items available there are rare occasions when an item has been uploaded in error or has been deemed to be commercially or otherwise sensitive.

If you believe that this is the case for this document, please contact UBIRA@lists.bham.ac.uk providing details and we will remove access to the work immediately and investigate.

1 **Organic characterisation of cave drip water by LC-OCD and fluorescence analysis**

2
3 Helen Rutledge,^{a,b,*} Martin S. Andersen,^c Andy Baker,^b Khorshed J. Chinu,^a Mark O.
4 Cuthbert,^{c,d} Catherine Jex,^b Christopher E. Marjo,^a Monika Markowska,^{b,e} Gabriel C. Rau^c

5
6 ^a Solid State and Elemental Analysis Unit, Mark Wainwright Analytical Centre, UNSW
7 Australia, Kensington, NSW, Australia 2052

8 ^b Connected Waters Initiative Research Centre, UNSW Australia, Kensington, NSW,
9 Australia 2052

10 ^c Connected Waters Initiative Research Centre, UNSW Australia, 110 King Street, Manly
11 Vale, NSW 2093, Australia

12 ^d School of Geography, Earth and Environmental Sciences, University of Birmingham,
13 Edgbaston, Birmingham, B15 2TT, UK

14 ^e Australian Nuclear Science and Technology Organisation, Lucas Heights NSW 2234,
15 Australia

16
17 * Corresponding author. Tel.: +612 8071 9864

18 E-mail address: h.rutledge@unsw.edu.au

19 20 **Abstract**

21 Cathedral Cave, Wellington, Australia, is a natural laboratory for studying water movement
22 and geochemical processes in the unsaturated zone by using artificial irrigation to activate
23 drip sites within the cave. Water sampled from two drip sites activated by irrigations carried
24 out in summer 2014 was analysed for dissolved inorganic ions and fluorescent organic
25 matter. The analysis allowed the development of a conceptual flow path model for each drip
26 site. DOM analysis was further complemented by liquid chromatography with organic carbon
27 detection (LC-OCD), applied for the first time to karst drip waters, allowing the
28 characterisation of six organic matter fractions. The differences in organic matter fractions at
29 each drip site are interpreted as a signature of the proposed flow paths. LC-OCD was also
30 compared with parallel factor analysis (PARAFAC) of the fluorescence and good correlations
31 were observed for high molecular weight organic matter. Strong positive correlations were
32 also observed for high molecular weight matter and Cu and Ni. This is suggestive of colloidal
33 transport of Cu and Ni by organic matter with high molecular weight, while small molecular
34 weight colloids were not efficient transporters. LC-OCD uniquely provides information on

35 non-fluorescent organic matter and can be used to further quantify drip water organic matter
36 composition.

37

38 **1. Introduction**

39 There has been increasing interest in dissolved organic matter (DOM) in cave drip water and
40 the potential use of organic markers in speleothems as paleoclimate proxies (Blyth et al.,
41 2008; Fairchild and Baker, 2012). While initial studies focussed on bulk organic matter
42 (Baker et al., 1997), subsequent investigations have focussed on the potential of lipid
43 biomarkers (Xie et al., 2003; Blyth et al., 2007; Rushdi et al., 2011), polycyclic aromatic
44 hydrocarbons (PAHs) (Perrette et al., 2013), $\delta^{13}\text{C}$ of organic matter (Blyth et al., 2013a, b)
45 and trace elements associated with organic colloids (Hartland et al., 2012; 2014). Lipids such
46 as n-alkanes have been shown to record vegetation and land-use change (Blyth et al., 2007;
47 2011) and glycerol dialkyl glycerol tetraethers have shown potential as a paleotemperature
48 proxy (Blyth and Schouten, 2013; Blyth et al., 2014).

49

50 Cave-based monitoring programs are typically utilised to understand the processes affecting
51 organic matter concentration and character as it is transported from the soil to the cave.
52 Typically cave drip water organic carbon concentrations are less than 3 mg/L (Baker et al.,
53 1997; Ban et al., 2008), and are likely to be more variable than groundwater (Shen et al.,
54 2014). This combined with relatively small water sample volumes that can be obtained from
55 stalagmite drip water means that unfeasibly large water sample volumes are required for most
56 biomolecular characterisation techniques. Apart from one study on drip water PAHs (Perrette
57 et al 2013) and one on LMW fatty acids (Bosle et al 2014), published drip water organic
58 matter monitoring has focussed on the measurement of the fluorescent organic matter fraction
59 (fDOM), as this requires about 4 mL of water sample, no pretreatment and has low detection
60 limits (Baker et al., 1997; Baker and Genty, 1999), however, this technique can only provide
61 information about the fluorescent fraction of the organic matter.

62

63 Liquid chromatography-organic carbon detection (LC-OCD) can be used to identify classes
64 of organic compounds in water samples. It gives quantitative information on natural organic
65 matter (NOM) and qualitative results regarding molecular size distribution of organic
66 impurities in water. The qualitative analysis is based on size exclusion chromatography
67 where large molecules have different degrees of interaction with the pores on the column
68 material resulting in different retention times for different molecular size fractions.

69 Quantification is completed by carbon mass determination, similar to total organic carbon
70 (TOC) analysis, performed with both UV and organic carbon IR detectors which enable DOC
71 quantification at the sub-ppm level with only small sample volumes (10 mL). The resulting
72 chromatograms have significantly overlapping peaks, which typically require manual
73 processing to obtain correct peak separation, and therefore the expert knowledge of the user
74 is important for reliable results. The technique is relatively new but has seen extensive use
75 characterising the efficiency of water treatment processes (Zheng et al., 2010; Li et al., 2012)
76 as well as natural organic matter (NOM) in fresh and marine waters (Velten et al., 2011;
77 Rachman et al., 2014).

78

79 The DOC comprises hydrophobic organic carbon (HOC) that has a strong hydrophobic
80 interaction with the column material and does not elute through the column and
81 chromatographic dissolved organic carbon (CDOC). The HOC is determined by difference
82 between total organic carbon, determined by bypass of the column, and the CDOC. The five
83 different groups of CDOC that can be fractionated by the column are biopolymers, humic
84 substances, building blocks, low molecular weight (LMW) acids and neutrals, details of these
85 fractions are given in Table 1. These compounds are characterized by a UV-detector ($\lambda = 254$
86 nm) and quantified by IR-detection after UV oxidation in a cylindrical UV thin-film reactor
87 (Huber et al., 2011).

88

89 The purpose of this study is to evaluate and compare LC-OCD and fluorescence analyses as a
90 tool for characterisation of DOM in cave drip waters, and to understand the time evolution of
91 organic matter fractions in the context of the routing of water between surface and drip site.

92

93 **2. Material and methods**

94 2.1 Study site

95 Cathedral Cave at Wellington Caves, NSW, Australia (32°37'S; 148°56'E) was used as the
96 location for this study (Figure 1). The geology of the region has previously been described
97 (Johnson, 1975) and the cave is within an area of massive Devonian limestone, with a thin-
98 layer of red-brown soil comprising clays, iron oxides, fine quartz sands, and calcite nodules
99 (Frank, 1971), with aeolian contributions (Hesse and McTanish, 2003). The site is within a
100 temperate semi-arid region, with mean annual precipitation of 619 mm (1956-2005) and
101 evaporation of 1825 mm (1956-2005) recorded at the nearby Wellington Research Centre

102 (Australia Bureau of Meteorology). There is a significant seasonal temperature variation with
103 monthly mean maximum ranging from 15 °C in July and 32 °C in January (1956-1990,
104 Australia Bureau of Meteorology).

105
106 The cave continues to be a focus of long-term hydrogeological monitoring (concurrent to this
107 study) by the investigators, commencing in 2010 and continuing, primarily using a network
108 of in-situ Stalagmate © drip loggers. Jex et al. (2012) described infiltration patterns and
109 processes within the cave, and identified that infiltration only occurs after high magnitude
110 and long duration rainfall events, with a total precipitation of over ~60 mm within 24-48
111 hours, however the necessary amount of rainfall needed can vary dependant on antecedent
112 soil conditions. Such rainfall events occur very infrequently, typically 0-2 times a year, and
113 require slow-moving weather systems. In winter, this is most likely associated with westerly
114 frontal rainfall, where the associated low pressure system is slow moving, deep, and
115 relatively close to the site. In summer, atmospheric instability and associated convective
116 rainfall caused by slow moving or stationary troughs and associated upper level systems,
117 draws moist, unstable air from the north of the region. Drip water isotope monitoring
118 demonstrated that drip water $\delta^{18}\text{O}$ is dominated by epikarst evaporation (Cuthbert et al.,
119 2014a). Due to the infrequent recharge events, evaporation from near-surface karst water
120 stores leads to increasingly enriched cave drip waters.

121
122 Most recently, Cathedral Cave has been utilised for regular artificial irrigation experiments,
123 to better understand karst hydrogeochemical processes. An irrigation in the summer of 2013
124 has been used to understand drip water trace element and organic matter hydrogeochemical
125 evolution during recharge events (Rutledge et al., 2014). An irrigation in the summer of 2014
126 has been used to understand the role of within-cave evaporation during recharge events, and
127 identified the role of evaporative cooling on drip waters for the first time (Cuthbert et al.,
128 2014b). Data from both irrigation experiments has been used to quantify the processes of heat
129 transport (Rau et al., 2015). The data presented here is from water samples collected during
130 the summer 2014 irrigation event.

131
132 2.2 Irrigation experiment
133 For this study, an area of approximately 5×10 m, directly above the study area in Cathedral
134 Cave was irrigated with Wellington town supply water. The experiment was performed at the

135 height of the Australian summer and the antecedent soil moisture was low (initial average soil
136 moisture was measured as 14.4 wt%). Two irrigations by hand hosing were performed on
137 consecutive mornings. The irrigation on Day 1 started at 7:50 am and continued for three
138 hours until dripping was initiated in the cave at five sites below the irrigation zone, one of
139 which had been used for drip water sampling previously and designated Site 1 (Rutledge et
140 al., 2014) (Figure 1). A total of 3400 L was applied. The irrigation on Day 2 comprised two
141 batches of irrigation water. The initial batch was 1000 L town water loaded into a tank on site
142 and spiked with 0.5 L of 99.8% deuterium (D₂O), resulting in a deuterium enrichment of
143 6700 ‰ (VSMOW) as measured by laser cavity ring down mass spectrometry (see below).
144 This batch was hand hosed for 1 ¾ hours then followed by a second non-enriched batch of
145 1430 L of town water for 1 ½ hours. Following this irrigation, an additional site activated and
146 was designated Site 25 (Figure 1). Site 1 was equipped with a Stalagmate® drip logger
147 during the experiment.

148

149 2.3 Sampling and in-cave measurements

150 For each drip water sample collected from Sites 1 and 25, a volume of 200-300 mL was
151 collected, which took approximately 30 minutes. Alkalinity, pH, electrical conductivity (EC)
152 and temperature were measured immediately after sampling. Alkalinity was determined on a
153 10 mL sub-sample using Gran titration with a 0.16 N H₂SO₄. Sub-samples for cation, anion,
154 fluorescence, LC-OCD and isotopic analysis were filtered (0.45 µm) and prepared for
155 subsequent laboratory testing, with the cation samples acidified with 2% 10 N nitric acid to
156 ensure stability during storage. In addition, one sample from each batch of irrigation water
157 (i.e. Day 1, Day 2 deuterium enriched and non-enriched town water) was collected for
158 analysis as above.

159

160 2.4 Trace element and anion analysis

161 Trace-element analysis of the drip water and each batch of irrigation water (without dilution)
162 was carried out using a Perkin Elmer NexION 300D ICP-MS and Perkin Elmer Optima 7300
163 ICP-OES. The following elements were analysed by ICP-OES: Ca, K, Mg, Na, Si and Sr, and
164 by ICP-MS: Al, Ba, Cu, Fe, Mn, Ni and Zn (Table EA1). The method has been described in
165 detail previously (Rutledge et al., 2014). In addition, a Dionex Ion chromatography system
166 was used to determine the concentration of the following anions, fluoride, chloride, nitrite,
167 bromine, nitrate, phosphate and sulfate. Of these only chloride, bromide and sulfate were

168 above the detection limit (Table EA2). PHREEQC for Windows (Parkhurst & Appelo, 2003)
169 was used to calculate saturation indices on selected minerals from the dissolved
170 concentrations.

171

172 2.5 Fluorescence analysis

173 Fluorescence excitation-emission matrices (EEM's) were obtained for the collected drip
174 water samples using a Horiba Aqualog fluorescence spectrometer. This spectrometer allows
175 for the collection of absorbance and fluorescence within the same instrument, with the
176 absorbance data used to correct for any reabsorption (or inner-filter) effects. Fluorescence
177 EEMs were collected using an excitation range of 240 to 400 nm, with a step-size of 3 nm,
178 and emitted fluorescence detected between 210 and 600 nm with a CCD detector, at a
179 spectral resolution of 1.64 nm and integration time of 1 s. All data was inner-filter corrected,
180 scatter lines masked, and Raman normalised (to a mean Raman intensity of water in a sealed
181 water cell, excited at 380 nm, of 200 intensity units), using proprietary Aqualog software.
182 The resultant dataset of 19 EEMs was analysed using a previous calibrated parallel factor
183 analysis (PARAFAC) model for this site (see Rutledge et al., 2014) using Eigenvector
184 Research Solo © software. These three factors were characterised, following Ishii and Boyer
185 (2012), as unprocessed, soil-derived humic-like and fulvic-like material (Factor 1),
186 biogeochemically processed humic/fulvic-like material (Factor 2), and living or dead
187 microbial matter (tryptophan-like fluorescence) (Factor 3) which is indicative of
188 microbiological activity (Hudson et al., 2007).

189

190 2.6 LC-OCD analysis

191 The LC-OCD is an automated size-exclusion chromatography system coupled to three
192 detectors, for organic carbon, organic nitrogen and UV absorbance, respectively. Details of
193 the measurement procedure have been described in full by Huber et al. (2011). In this study, a
194 Toyopearl TSK HW50S column was used with a phosphate buffer mobile phase of pH 6.4 at
195 a flow rate of 1.1 mL/min. Injection volumes were 1 mL. The chromatographic column is a
196 weak cation exchange column containing a polymethacrylate filter. The chromatography
197 subdivides into six sub-fractions, which are assigned to specific classes of compounds: that is
198 biopolymers, humics, building blocks, low molecular-weight neutrals and hydrophobic
199 organic carbon (Huber et al., 2011).

200

201 2.7 Deuterium analysis

202 The isotopic composition of irrigation and drip water samples were determined using an
203 LGR-100DT V2 off-axis, integrated cavity output, cavity ring-down mass-spectrometer
204 (Wassenaar et al., 2008; Cuthbert et al., 2014a) at UNSW Australia. Each sample was run
205 with a total of 10 injections and run in triplicate (total of 30 injections), with the average of
206 the replicates used as the reported value. Four internal reference standards provided by the
207 Australian Nuclear Science and Technology Organisation with deuterium values of: -174.1, -
208 78.8, -6.54, 32.3 ‰ VSMOW were used. An additional independent laboratory reference
209 standard was used from Elemental Microanalysis with deuterium value of 4.93 relative to
210 VSMOW. The analytical precision for deuterium were ~1.5‰ VSMOW (1 σ ; calculated from
211 within run internal reference materials). This compares to an external precision for deuterium
212 of 0.6‰ (1 σ , analysis of standards). The calibration curve was calculated using the reference
213 standards and was used to interpolate drip water and irrigation water samples. Samples which
214 fell outside of the range of the reference standards were extrapolated.

215

216 **3. Results**

217 Figure 2 shows the drip rate data for Site 1 over the course of the experiment. Dripping at
218 Site 1 activated on Day 1 and stopped on Day 3, while a secondary site, Site 25, activated on
219 Day 2 and continued on Day 3 and beyond. At Site 1, the two irrigations above the cave
220 resulted in two significant pulses, with a three hour delay on Day 1 and one hour delay on
221 Day 2 from the start of each irrigation. The second site considered in this study (Site 25) was
222 an unexpected activation on Day 2 in a relatively inaccessible location in the cave and no
223 measured drip rate data is available, however sampling for both sites was possible over the
224 course of the experiment allowing both sites to be chemically characterised. When dripping
225 had commenced at Site 25 it was observed to be consistent but at a lower frequency than the
226 initial activation at Site 1, suggesting there are flow restrictions at this site relative to Site 1.
227 Site 1 shows an overall higher pH, lower alkalinity and Ca concentration than Site 25. This is
228 reflected in the PHREEQC calculated PCO₂ and saturation indices for calcite that are both
229 lower for Site 1. Calculations indicate near saturation of calcite at Site 25 and a PCO₂ that is
230 an order of magnitude higher than at Site 1.

231

232 A previous study by the authors at this location established that certain elements were derived
233 predominantly from either the bedrock or the soil using a principal component analysis
234 (PCA) model (Rutledge et al., 2014). Ba, Cu and Ni were soil-derived elements and Ca and Sr
235 were limestone bedrock-derived elements. A soil source for both Ni and Cu is likely as they

236 are both organo-colloid associated trace elements (Hartland et al., 2012). Ba was not detected
237 in limestone bedrock samples and since it is strongly absorbed to clay minerals, the clay-rich
238 soils likely provide the dominant source of the Ba. Table 2 shows that at Site 1 the bedrock-
239 derived Ca concentration was lower than at Site 25, while the soil-derived elements of Ba, Cu
240 and Ni were higher. A relatively small difference was observed for Sr between the two sites.
241 While the initial concentrations of elements in irrigation water were comparable to the drip
242 water concentrations, irrigation water does not make a significant contribution to the
243 measured drip water concentrations due to dilution with existing stored water, based on the
244 deuterium measurements (see Table 2). A minimum dilution down to 3.5% can be estimated
245 based on the initial deuterium isotope ratio in the irrigation tank (6700‰ VSMOW) and the
246 maximum deuterium ratio measured at Site 1 of 220‰ VSMOW against the background
247 deuterium ratio of -13‰ VSMOW. The deuterium ratio measured at Site 25 (38‰ VSMOW
248 on average) is above the background level (assumed to be same as Site 1) but relatively
249 consistent and significantly lower than the maximum value for Site 1.

250

251

252

253 Figure 3 shows the behaviour of the PARAFAC factors derived from the analysis of the
254 fluorescent EEM data over the course of the study. The three factors characterised were
255 unprocessed, soil-derived humic-like and fulvic-like material (Factor 1), biogeochemically
256 processed humic/fulvic-like material (Factor 2), and living or dead microbial matter
257 (tryptophan-like fluorescence) (Factor 3). These three factors are the same as those observed
258 in the 2013 irrigation experiments (Rutledge et al., 2013). Overall the drip water from Site 1
259 contains more organic matter than Site 25. Factor 1 and Factor 2 show a relatively small
260 decrease between the two irrigations at Site 1. At Site 25 these factors are relatively constant.
261 Factor 3 (microbial-derived) shows initial high values for the first irrigation and then
262 decreasing for the second irrigation at Site 1 compared to Site 25 where it is relatively
263 unchanged.

264

265 Figure 4 shows the time-series concentration profiles for the organic fractions measured by
266 LC-OCD for both sites. Overall the DOC concentration at Site 1, as measured by LC-OCD,
267 decreased over the course of the study, while at Site 25 the DOC concentration was lower and
268 remained relatively unchanged. The DOC fraction comprises both HOC (hydrophobic) and
269 CDOC (hydrophilic) organic carbon. The CDOC fraction can be further broken down into

270 chemical fractions of bio-polymers, humics, building blocks and LMW neutrals. For both
271 sites the concentration of CDOC (Site 1 average was 4565 µg/L and Site 25 average was
272 2150 µg/L) was significantly higher than the HOC concentrations (the average values for Site
273 1 and Site 25 were 1213 µg/L and 736 µg/L respectively). In terms of individual fractions,
274 the bio-polymers decreased over time at Site 1 but were close to the detection limit at Site 25.
275 Building blocks were fairly consistent each day but showed a decrease from day to day at Site
276 1.

277
278 Table EA3 shows the Kendall tau correlations between selected elements and the LC-OCD
279 fractions. Ca (bedrock-derived) shows negative correlations with DOC (-0.61), CDOC (-0.61)
280 and humics (-0.66). While Cu and Ni (soil-derived) show positive correlations with all LC-
281 OCD fractions except building blocks and LMW neutrals. Ba shows positive correlations
282 with DOC (0.62) and humics (0.62).

283
284 Overall the irrigation water contains the highest proportion of CDOC (hydrophilic) followed
285 by Site 1, with Site 25 the lowest. Conversely, HOC (hydrophobic) showed the lowest
286 proportion in the irrigation water, increasing in Site 1 and again in Site 25. There are clear
287 differences in the relative proportions of the different hydrophilic fractions measured by LC-
288 OCD in the DOC of the irrigation water and the drip water from the two sites as shown in
289 Figure 5. Site 1 has higher proportion of humics, building blocks & bio-polymers while Site
290 25 has a higher proportion of LMW neutrals. Site 25 shows the most difference from the
291 irrigation water.

292 293 **4. Discussion**

294 4.1 Flow path Model

295 After the first irrigation dripping at Site 1 responded within 3 hours, with an initial high drip
296 rate decreasing over 20 hours. This ‘flashy’ flow response, in combination with a short arrival
297 time for the deuterium tracer, suggests a short flow path for Site 1. This is supported by an
298 excavation that revealed a soil filled void in the limestone directly above Site 1, and a
299 measured maximum bedrock thickness of only ~ 1.5 m. In comparison, Site 25 showed a
300 lagged and damped flow response and deuterium tracer breakthrough, suggesting a
301 combination of more unsaturated zone storage water, tortuous/longer pathways through the
302 epikarst and lower fracture permeability. Deuterium measurements at both sites showed
303 significant dilution by existing stores of water. Site 25 showed a higher level of dilution of

304 the tracer (down to 0.9%) compared to Site 1 (down to 3.5%), suggesting that the Site 25
305 store contained more water. This increased dilution can partly explain the decreased total
306 DOC observed at Site 25 compared to Site 1.

307

308 Since cave drip water carries a chemical signature indicative of its flow path, the analysis
309 provided here can be used to reveal characteristics of flow routing between surface and cave.
310 Our interpretation benefits from the long-term drip water isotope monitoring program at the
311 cave (Cuthbert et al 2014a). That study demonstrated the ubiquitous presence of enriched drip
312 water isotopes, that could only be explained by evaporation from water stored in fractures or
313 voids the shallow vadose zone. Site 1 has PCO_2 values (Figure 2) only slightly elevated
314 above atmospheric values that could indicate poor CO_2 production in the soil, loss of
315 produced CO_2 by ventilation, or degassing as the water flowed down over the exposed
316 flowstone surface between the exfiltration point and drip site. Site 25 on the other hand had
317 PCO_2 values about one order of magnitude above those of Site 1 due to longer residence
318 times in the bedrock and a more restricted pore space minimising CO_2 loss to the atmosphere.
319 The recorded pH values largely reflect the calculated PCO_2 values, but may be tempered by
320 calcite dissolution (hence the near neutral pH values). Calcium, alkalinity and the saturation
321 index (SI) for calcite indicate that water sampled at Site 25 is more ‘evolved’ since it is closer
322 to equilibrium with calcite. It further indicates that there was a larger volume of stored water
323 in the flow path connecting to Site 25. Conversely at Site 1, the inorganic carbon
324 observations suggest that there is lower volume of stored water and that the store is in the soil
325 above the limestone. This is supported by higher concentrations of trace elements at Site 1
326 previously shown to be associated with soil at this study location, specifically Ba, Cu and Ni
327 (Rutledge et al., 2014).

328

329 Figure 6 shows a proposed schematic of flow paths for Sites 1 and 25 derived from the
330 observations above. In summary, Site 1 drip water travels through a void in the bedrock that
331 was filled with partially saturated soil, followed by further passage through a relatively thin
332 (<1.5m) amount of limestone, before entering the cave near the cave roof. The water
333 continues to flow over the cave wall, forming a flowstone deposit, before dripping from a
334 stalactite at Site 1. . Site 25 is fed by a long thin bedrock fracture, or a series of fractures,
335 which requires more water to enter the epikarst and/or more time than Site 1 before activating
336 the drip point.

337

338 4.2 Correlations between PARAFAC, LC-OCD and trace elements

339 The site had experienced a total of only 88 mm of rainfall over six events in the three months
340 prior to the irrigation and as a result the volume of water required to overcome the soil
341 moisture deficit and activate dripping was at least 1500 L. This volume of water was only
342 available from the local town water supply where DOM is present at comparable levels to
343 those measured in the drip water. Hence, DOM in the drip water will be derived from existing
344 DOM in town water and DOM extracted from soil organic matter in the epikarst. However,
345 as with the trace elements the DOM in the irrigation water would be diluted by the existing
346 water stored in the epikarst.

347

348 Figure 7 shows plots of selected LC-OCD derived classes of compounds that can be related
349 to the three corresponding PARAFAC factors from all samples taken over the course of the
350 study. Factor 1, unprocessed humic and fulvic acids, shows a strong correlation with the LC-
351 OCD humic fraction (Kendall tau coefficient of 0.61), as does Factor 2 (Kendall tau
352 coefficient of 0.79), which is processed humic and fulvic acids. The LC-OCD humic fraction
353 therefore correlates with the two PARAFAC factors which are also associated with humic-
354 like material, with the PARAFAC analysis suggesting that the LC-OCD humic fraction
355 comprises two different optical components. Factor 3 shows the highest correlation with bio-
356 polymers (Kendall tau coefficient of 0.69). Factor 3 is characterised as tryptophan-like
357 fluorescence, typically derived from living or dead microbial matter, and the correlation with
358 bio-polymers suggests a microbial biopolymer source. In addition to the plots shown in Figure
359 6, Factor 1 and 2 are positively correlated with DOC measured by LC-OCD, and the HOC
360 (hydrophobic) and CDOC (hydrophilic) LC-OCD fractions (see Table EA3). Factor 1 is also
361 positively correlated with the derived aromaticity index and Factor 2 with the building block
362 fraction. In most cases the LC-OCD derived indices, aromaticity, molecular weight, inorganic
363 colloids and specific UV absorbance (SUVA) did not show strong correlations with any
364 PARAFAC factors or LC-OCD fractions. The correlations observed in Figure 7 demonstrate
365 that LC-OCD agrees with the PARAFAC factor assignments from the fluorescence analysis.

366

367 LC-OCD uniquely provides information on non-fluorescent organic matter and can be used to
368 identify and quantify changes in organic matter composition. Figure 8 shows individual
369 scatter plots of the LC-OCD fractions and HOC (hydrophobic) expressed in terms of percent
370 of total DOC, to minimise the changes due to dilution. LMW neutrals are relatively higher at
371 Site 25 than Site 1 indicating that they are highly mobile and eluted rapidly as expected for

372 uncharged low molecular weight DOM (Shen et al., 2014). In contrast building blocks are
373 relatively lower at Site 25 compared to Site 1 which suggests that they are interacting with
374 the calcite surface in the epikarst (Alipour Tabrizy et al. 2011; Suess, 1970 and Suess, 1973).

375

376 Drip water from Site 25 consistently contained low levels of biopolymer and were often
377 below detection. Along with the correlation with PARAFAC Factor 3, this suggests that there
378 was an initial flush of biopolymer at Site 1 that would be expected to have accumulated in the
379 partially saturated lower soil layer prior to the first irrigation. The LC-OCD biopolymer
380 fraction is defined as being >20 kDa and hydrophilic (Huber et al 2011) organic compounds
381 such as polysaccharides. We hypothesise that the longer flow path at Site 25 leads to greater
382 loss of this fraction, for example by microbial degradation, compared to Site 1.

383

384 The relative decrease in the humic substances fraction at Site 25 can be explained by the
385 preferential adsorption of the negatively charged humic fraction at the positively charged
386 calcite surface during flow through the bedrock fracture. We observe ongoing calcite
387 formation in the form of active flowstone deposits (Site 1) and stalactite formation (Sites 1
388 and 25). Ongoing calcite formation from solution provides a continual source of fresh
389 surfaces that are positively charged at the drip water pH (approximately 8), below the point of
390 zero charge of calcite, $\text{pH}_{\text{PZC}} = 9.5$ (Appelo and Postma, 2005). This preferential adsorption
391 is supported by numerous laboratory studies of organic matter interaction with calcite
392 (Alipour Tabrizy et al. 2011; Suess, 1970 and Suess, 1973). LC-OCD therefore helps identify
393 changes in organic matter composition, with loss of different organic matter fractions due to
394 processes which include sorption and microbial processing. Such changes in composition can
395 be conceived as a smaller-scale manifestation of the “regional scale chromatography”
396 proposed for groundwater (Hedges et al., 1986; Shen et al., 2014).

397

398 Strong positive correlations were observed for Cu and Ni with the higher molecular weight
399 LC-OCD fractions, for example biopolymers-Cu (0.76) and humics-Ni (0.80). This supports
400 a prior study by Hartland et al (2012) who used flow field-flow fractionation of karst drip
401 waters that showed colloidal transport of Cu and Ni by organic matter with high molecular
402 weight. This same study observed that small molecular weight colloids were not efficient
403 transporters of Cu and Ni, and we further confirm this observation here as we see low
404 correlations observed for these elements and the LMW neutrals (0.40 and 0.24, respectively).
405 We also considered the relationship between the Cu/Ni ratio and LC-OCD fractions and

406 derived indices (Table EA3 and Figure 9). Hartland et al (2012) have previously hypothesised
407 that the Cu/Ni ratio in cave drip waters is indicative of a quality change in DOM, as Cu has
408 an increased affinity to binding to aromatic binding sites than Ni. For the whole dataset
409 (Table EA2), our results show that the only statistically significant correlation between Cu/Ni
410 and LC-OCD fractions is a negative correlation with humics (-0.49) and we see no significant
411 correlations between Cu/Ni and the derived indices of molecular weight or aromaticity.
412 However, at a site-by-site basis (Figure 9), we observe that these global correlations are
413 masking site-specific patterns. At Site 1, there are positive correlations between Cu/Ni and
414 aromaticity and molecular weight, as predicted by Hartland et al (2012), and also with
415 building blocks and LMW neutrals. In contrast, correlations between Cu/Ni and LC-OCD
416 fractions and derived indices are very weak at Site 25, but the site as a whole has high Cu/Ni
417 than Site 1, which explains the global negative correlations observed (Table EA2). Our LC-
418 OCD results suggest a complex relationship between organic matter character as determined
419 by LC-OCD and Cu/Ni over the event timescale which requires further investigation.

420

421 Compared with fluorescence analysis LC-OCD provides more information on the types of
422 colloid-forming DOM involved in metal transport. Our results that demonstrate correlation
423 between Cu and Ni concentration and DOM concentration for all data, but only with the
424 largest size fractions (humics and biopolymers). The correlation between Cu/Ni and
425 aromaticity varies between the two sites. It is strongest at Site 1, despite the lack of
426 correlation between humic fraction concentration and Cu/Ni, confirming an aromaticity
427 control on Cu/Ni (Hartland et al. 2012). However, variations in the correlation with LC-OCD
428 fractions and indices between flow paths and within recharge events suggest that flow
429 switching and discharge variability may be preserved in speleothem records of these organic-
430 transported metals.

431 **5. Conclusions**

432 Trace element composition measured by ICP and organic matter analysis by fluorescence has
433 been applied to cave drip water samples collected after a series of artificial irrigations. This
434 revealed an understanding of the flow paths feeding two drip sites. We propose that Site 1 is
435 fed by a short and permeable bedrock fracture via a soil store which retains relatively high
436 moisture content during periods of no rainfall. In comparison the data suggest that Site 25 is
437 fed by an area of thinner, drier soil through a thicker epikarst with greater unsaturated storage
438 and/or lower permeability.

439

440 DOM analysis was also performed by LC-OCD, applied for the first time to karst drip waters.
441 Good correlations were observed between LC-OCD humic and bio-polymer fractions and the
442 corresponding PARAFAC factors from the fluorescent analysis. LC-OCD enabled a more
443 detailed characterisation of the non-fluorescent fractions of DOM present in the drip water
444 sample. LC-OCD identified that as the drip water moves through bedrock fractures there are
445 changes in dissolved organic matter composition which will depend on the path-length of the
446 water. Locations nearer the surface with shorter path-length and higher discharge have higher
447 DOC, as there is less time for organic matter sorption and microbial processing. At Site 25,
448 with the longer path-length, this leads to the preferential adsorption of the humic substance
449 fraction, resulting in a relative decrease in the hydrophilic portion of DOM compared to Site
450 1, while the uncharged low molecular weight neutrals pass through unaffected.

451

452 LC-OCD provides insights into vadose zone processes affecting dissolved organic matter,
453 such as sorption and microbial processing, which occur between different flow paths, within
454 discharge events and between discharge events. The greater level of chemical detail, unique
455 to LC-OCD, demonstrates its potential for providing insight into the evolution of organic
456 matter from soil to cave, through different flow paths in the unsaturated zone. An improved
457 understanding of these processes could have implications for selecting speleothem samples
458 suitable for biomarker research, such as when using lipids for paleoclimate reconstructions
459 (Blyth et al., 2007) or fluorescent organic matter to construct fluorescence lamina growth
460 chronologies (Baker et al., 1993). Research presented here, focusing on just two drip waters
461 of contrasting flow path-length, needs to be extended for a wider range of drip sites and caves
462 using LC-OCD.

463

464 **5. Acknowledgements**

465 We thank the staff at Wellington Caves for their support. Funding for this research was
466 provided by the National Centre for Groundwater Research and Training, an Australian
467 Government initiative, supported by the Australian Research Council and the National Water
468 Commission and Mark Wainwright Analytical Centre at UNSW Australia. Mark Cuthbert
469 was supported by Marie Curie Research Fellowship funding from the European Community's
470 Seventh Framework Programme [FP7/2007-2013] under grant agreement n°299091. We also
471 acknowledge the anonymous reviewers that provided helpful feedback.

472

473 **6. References**

474
475 Alipour Tabrizy, V., Denoyel, R. and Hamouda, A.A. (2011). Characterization of wettability
476 alteration of calcite, quartz and kaolinite: Surface energy analysis. *Colloids and Surfaces*
477 *A: Physicochemical and Engineering Aspects* **384**, 98-108.

478 Appelo, C.A.J. and Postma, D. (2005). *Geochemistry, Groundwater, and Pollution*, second
479 ed. A.A. Balkema, Rotterdam, 649 pp.

480 Baker, A., Smart, P. L., Edwards, R. L., and Richards, D. A. (1993). Annual growth banding
481 in a cave stalagmite. *Nature*, **364**, 518-520.

482 Baker, A., Barnes, W.L. and Smart, P.L. (1997). Stalagmite Drip Discharge and Organic
483 Matter Fluxes in Lower Cave, Bristol. *Hydrological Processes* **11**, 1541-1555.

484 Baker, A. and Genty, D. (1999). Fluorescence wavelength and intensity variations of cave
485 waters. *Journal of Hydrology* **217**, 19-34.

486 Ban, F., Pan, G., Zhu, J., Cai, B., and Tan, M. (2008). Temporal and spatial variations in the
487 discharge and dissolved organic carbon of drip waters in Beijing Shihua Cave, China.
488 *Hydrological Processes* **22**, 3749-3758.

489 Blyth, A.J., Asrat, A., Baker, A., Gulliver, P., Leng, M.J. and Genty, D. (2007). A new
490 approach to detecting vegetation and land-use change using high-resolution lipid
491 biomarker records in stalagmites. *Quaternary Research* **68**, 314-324.

492 Blyth, A.J., Baker, A., Collins, M.J., Penkman, K.E.H., Gilmour, M.A., Moss, J.S., Genty, D.
493 and Drysdale, R.N. (2008). Molecular organic matter in speleothems and its potential as an
494 environmental proxy. *Quaternary Science Reviews* **27**, 905-921.

495 Blyth, A.J., Thomas, L.E., Calsteren, P.V. and Baker, A. (2011). A 2000 year lipid biomarker
496 record preserved in a stalagmite from NW Scotland. *Journal of Quaternary Science* **26**,
497 326-334.

498 Blyth, A.J., Shutova, Y. and Smith, C.I. (2013). $\delta^{13}\text{C}$ analysis of bulk organic matter in
499 speleothems using liquid chromatography–isotope ratio mass spectrometry. *Organic*
500 *Geochemistry* **55**, 22-25.

501 Blyth, A.J., Smith, C.I. and Drysdale, R.N. (2013). A new perspective on the $\delta^{13}\text{C}$ signal
502 preserved in speleothems using LC-IRMS analysis of bulk organic matter and compound
503 specific stable isotope analysis. *Quaternary Science Reviews* **75**, 143-149.

504 Blyth, A.J. and Schouten, S. (2013). Calibrating the glycerol dialkyl glycerol tetraether
505 temperature signal in speleothems. *Geochimica Cosmochimica Acta* **109**, 312-328.

506 Blyth, A.J., Jex, C., Baker, A., Khan, S.J. and Schouten, S. (2014). Contrasting distributions
507 of glycerol dialkyl glycerol tetraethers (GDGTs) in speleothems and associated soils.
508 *Organic Geochemistry* **69**, 1-10.

509 Bosle, J.M., Mischel, S.A., Schulze A.-L., Scholz, D. and Hoffman, T. (2014) Quantification
510 of low molecular weight fatty acids in cave drip water and speleothems using HPLC-ESI-
511 IT/MS – development and validation of a selectiv emethod. *Anal. Bioanal. Chem.*, **406**,
512 3167-3177.

513 Cuthbert, M.O., Baker, A., Jex, C.N., Graham, P.W., Treble, P.C., Andersen, M.S. and
514 Acworth, R.I. (2014a). Drip water isotopes in semi-arid karst: Implications for speleothem
515 paleoclimatology, *Earth and Planetary Science Letters* **395**, 194-204.

516 Cuthbert, M.O., Rau, G.C., Andersen, M.S., Roshan, H., Rutledge, H., Marjo, C.E.,
517 Markowska, M., Jex, C.N., Graham, P.W., Mariethoz, G. Acworth, R.I. and Baker, A.
518 (2014b). Evaporative cooling of speleothem drip water. *Scientific Reports* **4**, .

519 Fairchild I. J. and Baker A. (2012) *Speleothem Science*. Wiley-Blackwell, 432 pp.

520 Frank, R. (1971). The clastic sediments of the Wellington Caves, New South Wales. *Helictite*
521 **9**, 3-26.

522 Hartland, A., Fairchild, I.J., Lead, J.R., Borsato, A., Baker, A., Frisia, S. and Baalousha, M.
523 (2012). From soil to cave: transport of trace metals by natural organic matter in cave
524 dripwaters. *Chemical Geology* **304-305**, 68-82.

525 Hartland, A., Fairchild, I.J., Müller, W. and Dominguez-Villar, D. (2014). Preservation of
526 NOM-metal complexes in a modern hyperalkaline stalagmite: Implications for speleothem
527 trace element geochemistry. *Geochimica et Cosmochimica Acta* **128**, 29-43.

528 Hedges, J.I., Ertel, J.L., Quay, P.D., Grootes, P.M., Richey, J.E., Devol A.H., Farewell G.W.,
529 Schmidt, F.W., and Salati, E. (1986). Organic carbon-14 in the Amazon River system.
530 *Science* **231**, 1129-1131.

531 Hesse P.P. and McTanish, G.H. (2003). Australian dust deposits: modern processes and the
532 Quaternary record. *Quaternary Sciences Reviews* **22**, 2007-2035.

533 Huber, S.A., Balz, A., Abert, M. and Pronk, W. (2011). Characterisation of aquatic humic
534 and non-humic matter with size-exclusion chromatography – organic carbon detection –
535 organic nitrogen detection (LC-OCD-OND). *Water Research* **45**, 879-885.

536 Hudson, N., Baker, A., Ward, D., Reynolds, D.M., Brunsdon, C., Carliell-Marquet, C. and
537 Browning, S. (2008). Can fluorescence spectrometry be used as a surrogate for the
538 Biochemical Oxygen Demand (BOD) test in water quality assessment? An example from
539 South West England. *Science of the Total Environment* **391**, 149-158.

540 Ishii S. K. and Boyer T. H. (2012). Behavior of reoccurring PARAFAC components in
541 fluorescent dissolved organic matter in natural and engineered systems: A critical review.
542 *Environmental Science and Technology* **46**, 2006–2017.

543 Jex C. N., Mariethoz G., Baker A., Graham P., Andersen M. S., Acworth I., Edwards N. and
544 Azcurra C. (2012). Spatially dense drip hydrological monitoring and infiltration behaviour
545 at the Wellington Caves, South East Australia. *International Journal of Speleology*. **41**,
546 285–298.

547 Johnson, B.D. (1975). The Garra Formation (early Devonian) at Wellington, N.S.W. *Journal*
548 *and Proceedings of The Royal Society of New South Wales* **108**, 111-118.

549 Li, S., Heijman, S.G.J., Verberk, J.Q.J.C., Verliefde, A.R.D., Amy, G.L. and van Dijk, J.C.
550 (2012). Removal of different fractions of NOM foulants during demineralized water
551 backwashing. *Separation and Purification Technology* **98**, 186-192.

552 Parkhurst, D. L. and Appelo C. A. J. (2003). PHREEQC for Windows: A Computer Program
553 for Speciation, Batch-Reaction, One-Dimensional Transport, and Inverse Geochemical
554 Calculations;[2.8. 03]. USGC, Washington, DC.

555 Perrette, Y., Poulenard, J., Durand, A., quiers, M., Malet, E., Fanget, B and Naffrechoux E.
556 (2013) Atmospheric sources and soil filtering of PAH content in karst seepage waters.
557 *Organic Geochemistry* **65**, 37-45

558 Rachman, R.M., Li, S., Missimer, T.M. (2014). SWRO feed water quality improvement using
559 subsurface intakes in Oman, Spain, Turks and Caicos Islands, and Saudi Arabia.
560 *Desalination*, **351**, 88-100.

561 Rau, G.C., Cuthbert , M.O., Andersen, M.S., Baker, A., Rutlidge, H., Markowska, M.,
562 Roshan, H., Marjo, C.E., Graham, P.W. and Acworth, R.I (2015). Controls on cave drip
563 water temperature and implications for speleothem based paleoclimate reconstructions.
564 *Quaternary Science Reviews*, in press.

565 Rushdi, A.I., Clark, P.U., Mix, A.C., Ersek ,V., Simoneit, B.R.T., Cheng, H. and Edwards,
566 R.L. (2011). Composition and sources of lipid compounds in speleothem calcite from
567 southwestern Oregon and their paleoenvironmental implications. *Environmental Earth*
568 *Sciences* **62**, 1245-1261.

569 Rutlidge, H., Baker, A., Marjo, C.E., Andersen, M.S., Graham, P.W., Cuthbert, M.O., Rau,
570 G.C., Roshan, H., Markowska, M., Mariethoz, G. and Jex, C.N. (2014). Dripwater organic
571 matter and trace element geochemistry in a semi-arid karst environment: Implications for
572 speleothem paleoclimatology. *Geochimica et Cosmochimica Acta* **135**, 217-230.

- 573 Shen, Y., Chapelle, F.H., Strom, E.W., and Benner R. (2014). Origins and bioavailability of
574 dissolved organic matter in groundwater. *Biogeochemistry* DOI 10.1007/s10533-014-
575 0029-4.
- 576 Suess, E. (1970). Interaction of organic compounds with calcium carbonate—I. Association
577 phenomena and geochemical implications. *Geochimica et Cosmochimica Acta* **34**, 157-
578 168.
- 579 Suess, E. (1973). Interaction of organic compounds with calcium carbonate-II. Organo-
580 carbonate association in recent sediments. *Geochimica et Cosmochimica Acta* **37**, 2435-
581 2447.
- 582 Velten, S., Knappe, D.R.U., Traber, J., Kaiser, H-P., von Gunten, U., Boller, M. and Meylan,
583 S. (2011). Characterization of natural organic matter adsorption in granular activated
584 carbon adsorbers. *Water Research* **45**, 3951-3959.
- 585 Xie, S., Yi, Y., Huang, J., Hu, C., Cai, Y., Collins, M. and Baker A. (2003). Lipid distribution
586 in a subtropical southern China stalagmite as a record of soil ecosystem response to
587 paleoclimate change. *Quaternary Research* **60**, 340-347.
- 588 Zheng, X.; Ernst, M., Jekel, M. (2010). Pilot-scale investigation on the removal of organic
589 foulants in secondary effluent by slow sand filtration prior to ultrafiltration. *Water*
590 *Research* **44**, 3203-3213.

591

592 **Captions**

593 Table 1: The fractions and derived indices obtained from LC-OCD.

594

595 Table 2: Average trace element concentrations for the irrigation water and Site 1 and 25.

596 Irrigation contribution is the estimated concentration of elements from the irrigation water to
597 the cave drip water after dilution by existing water stored in the vadose zone based on
598 deuterium measurements.

599

600 Figure 1 : Plan view of the study site at Cathedral Cave, Wellington Caves (top), with a
601 boxed area indicating the surface irrigation area and cave locations of the drip sites (adapted
602 from Sydney University Speleology Society survey map 2006-2007). The study site is in the
603 state of New South Wales in south eastern Australia (bottom).

604

605 Figure 2: Drip rate data (Site 1 only), deuterium, pH, alkalinity, Ca, LogPCO₂ and saturation
606 index for calcite (Sites 1 and 25) for the irrigation water and drip water samples. Grey
607 vertical bars indicate the irrigation periods. Lines between datapoints indicate periods of
608 continuous dripping.

609

610 Figure 3: PARAFAC factors 1-3 over time from the analysis of the fluorescence EEM data.
611 Lines between datapoints indicate periods of continuous dripping.

612

613 Figure 4: Time series of LC-OCD fractions for both sites. Lines between datapoints indicate
614 periods of continuous dripping.

615

616 Figure 5: Average composition of the DOC fraction for the irrigation water and both sites.

617

618 Figure 6: Simplified schematic of the different flow paths (prior to irrigation) derived from
619 the chemical signature of the drip water. The width of markers on each axis corresponds to
620 one metre.

621

622 Figure 7: PARAFAC factors versus selected LC-OCD fractions.

623

624 Figure 8: Matrix scatter plot of the percent of DOC of the LC-OCD fractions.

625

626 Figure 9: Matrix scatter plot of Cu/Ni against the LC-OCD fractions and indices.

606 Xie, S., Yi, Y., Huang, J., Hu, C., Cai, Y., Collins, M. and Baker A. (2003). Lipid distribution
607 in a subtropical southern China stalagmite as a record of soil ecosystem response to
608 paleoclimate change. *Quaternary Research* **60**, 340-347.
609 Zheng, X.; Ernst, M., Jekel, M. (2010). Pilot-scale investigation on the removal of organic
610 foulants in secondary effluent by slow sand filtration prior to ultrafiltration. *Water*
611 *Research* **44**, 3203-3213.

612

613 **Captions**

614 Table 1: The fractions and derived indices obtained from LC-OCD.

615

616 Table 2: Average trace element concentrations for the irrigation water and Site 1 and 25.
617 Irrigation contribution is the estimated concentration of elements from the irrigation water to
618 the cave drip water after dilution by existing water stored in the vadose zone based on
619 deuterium measurements.

620

621 Figure 1 : Plan view of the study site at Cathedral Cave, Wellington Caves (top), with a
622 boxed area indicating the surface irrigation area and cave locations of the drip sites (adapted
623 from Sydney University Speleology Society survey map 2006-2007). The study site is in the
624 state of New South Wales in south eastern Australia (bottom).

625

626 Figure 2: Drip rate data (Site 1 only), deuterium, pH, alkalinity, Ca, LogPCO₂ and saturation
627 index for calcite (Sites 1 and 25) for the irrigation water and drip water samples. Grey
628 vertical bars indicate the irrigation periods. Lines between datapoints indicate periods of
629 continuous dripping.

630

631 Figure 3: PARAFAC factors 1-3 over time from the analysis of the fluorescence EEM data.
632 Lines between datapoints indicate periods of continuous dripping.

633

634 Figure 4: Time series of LC-OCD fractions for both sites. Lines between datapoints indicate
635 periods of continuous dripping.

636

637 Figure 5: Average composition of the DOC fraction for the irrigation water and both sites.

638

Table1

		Description
Fraction	Biopolymers	Organic matter with high molecular weight, including polysaccharides, proteins and aminosugers. (Molecular weight > 20 kDa)
	Humics	Mixture of acids containing carboxyl and phenolate groups produced by biodegradation of dead organic matter. (Molecular weight ~ 1000 Da)
	Building blocks	Molecular chains of polyphenolics/polyaromatic acids that have deaggregated, due to breakage of hydrogen bonding and electrostatic interactions. (Molecular weight 300 – 500 Da)
	Low molecular weight (LMW) acids	Representing protic organic acids. (Molecular weight < 350 Da)
	Low molecular weight (LMW) neutrals	Uncharged small organics, including LMW alcohols, aldehydes, ketones, sugars and LMW amino acids. (Molecular weight < 350 Da)
	Hydrophobic organic carbon (HOC)	Fraction of DOC remaining in the column, implying a strong hydrophobic interaction with the column material, comprising longer chain aliphatic and polycyclic aromatic material.
Index	Aromaticity	Aromaticity provides an estimation of the degree of aromatic and unsaturated structures of the humic fraction.
	Molecular weight	A derived value of average molecular mass of the humic fraction.
	Inorganic colloids	Negatively charged inorganic polyelectrolytes, polyhydroxides and oxidhydrates of Fe, Al, S or Si, detected by UV light-scattering.
	SUVA	An additional parameter derived from the ratio of DOC and spectral absorption coefficient.

Table 2: Average trace element concentrations for the irrigation water and Site 1 and 25. Irrigation contribution is the estimated concentration of elements from the irrigation water to the cave drip water after dilution by existing water stored in the vadose zone based on deuterium measurements.

	Ca	Sr	Ba	Cu	Ni
	mg/L	mg/L	µg/L	µg/L	µg/L
Irrigation	26.93	0.18	59.71	1.32	0.67
Irrigation contribution	0.90	0.006	2.00	0.04	0.02
Site 1	97.68	0.07	10.77	0.90	0.26
Site 25	116.73	0.06	8.77	0.21	0.05

Figure1

[Click here to download high resolution image](#)

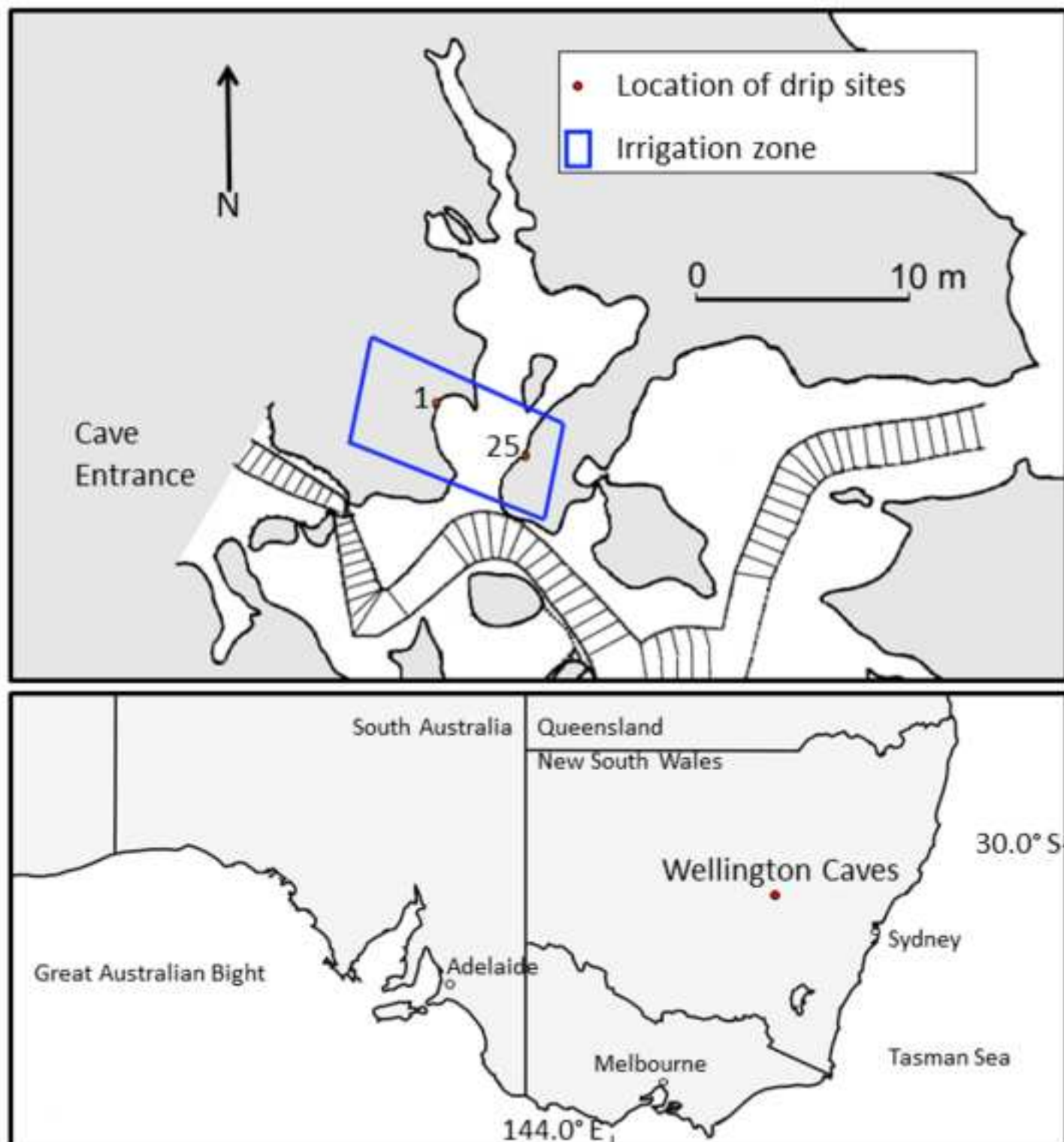


Figure2
[Click here to download high resolution image](#)

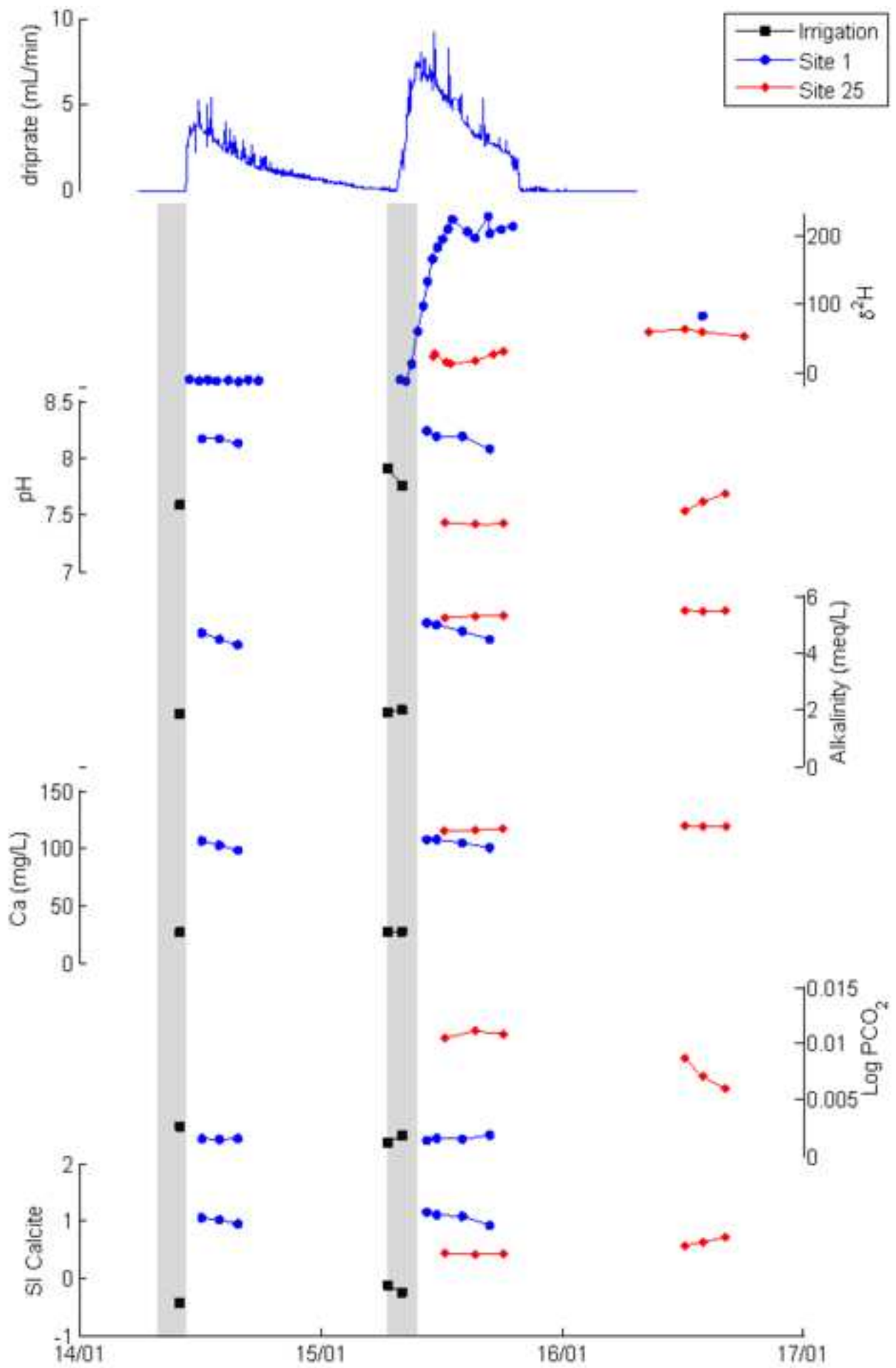


Figure3
[Click here to download high resolution image](#)

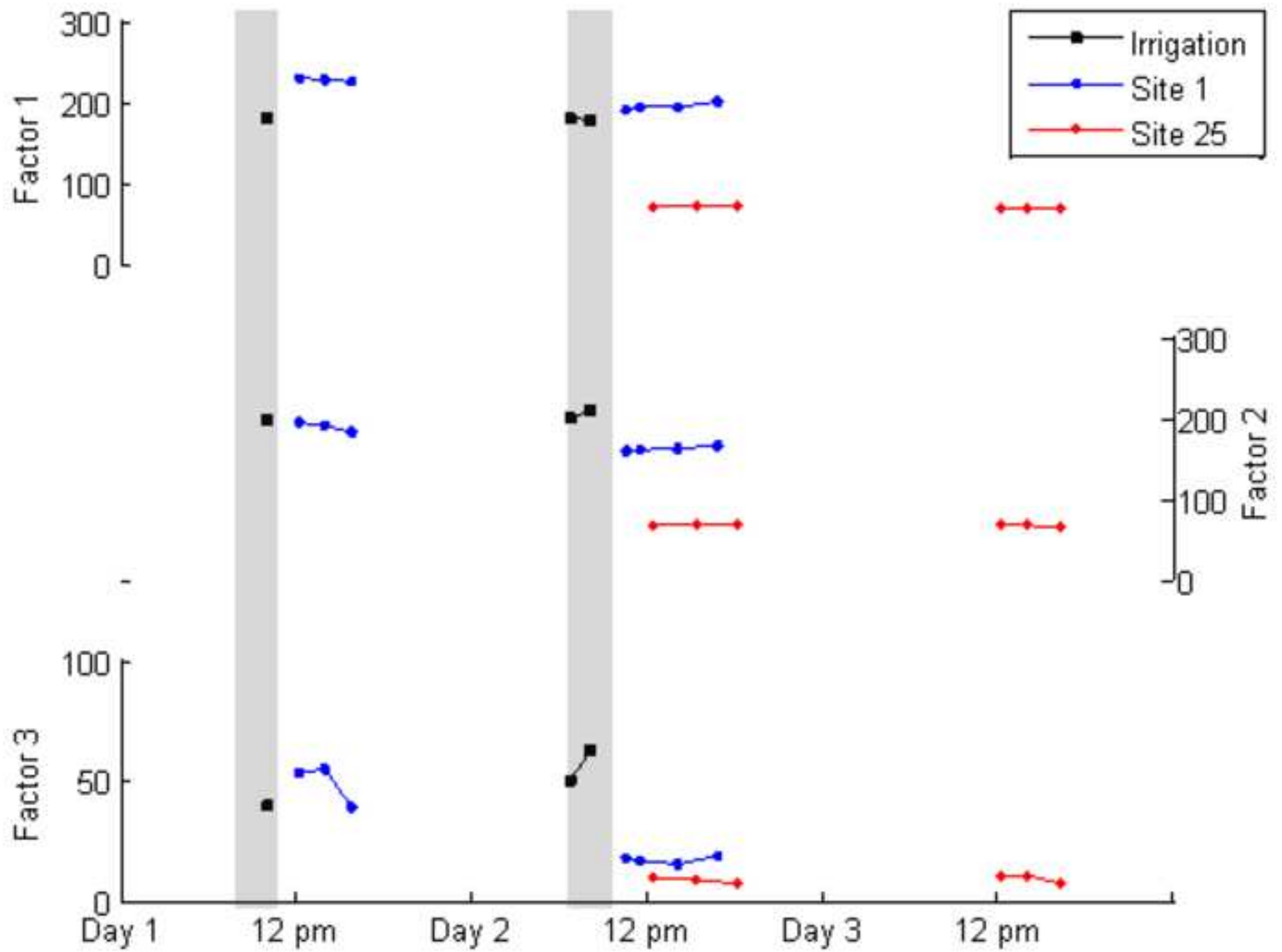


Figure4
[Click here to download high resolution image](#)

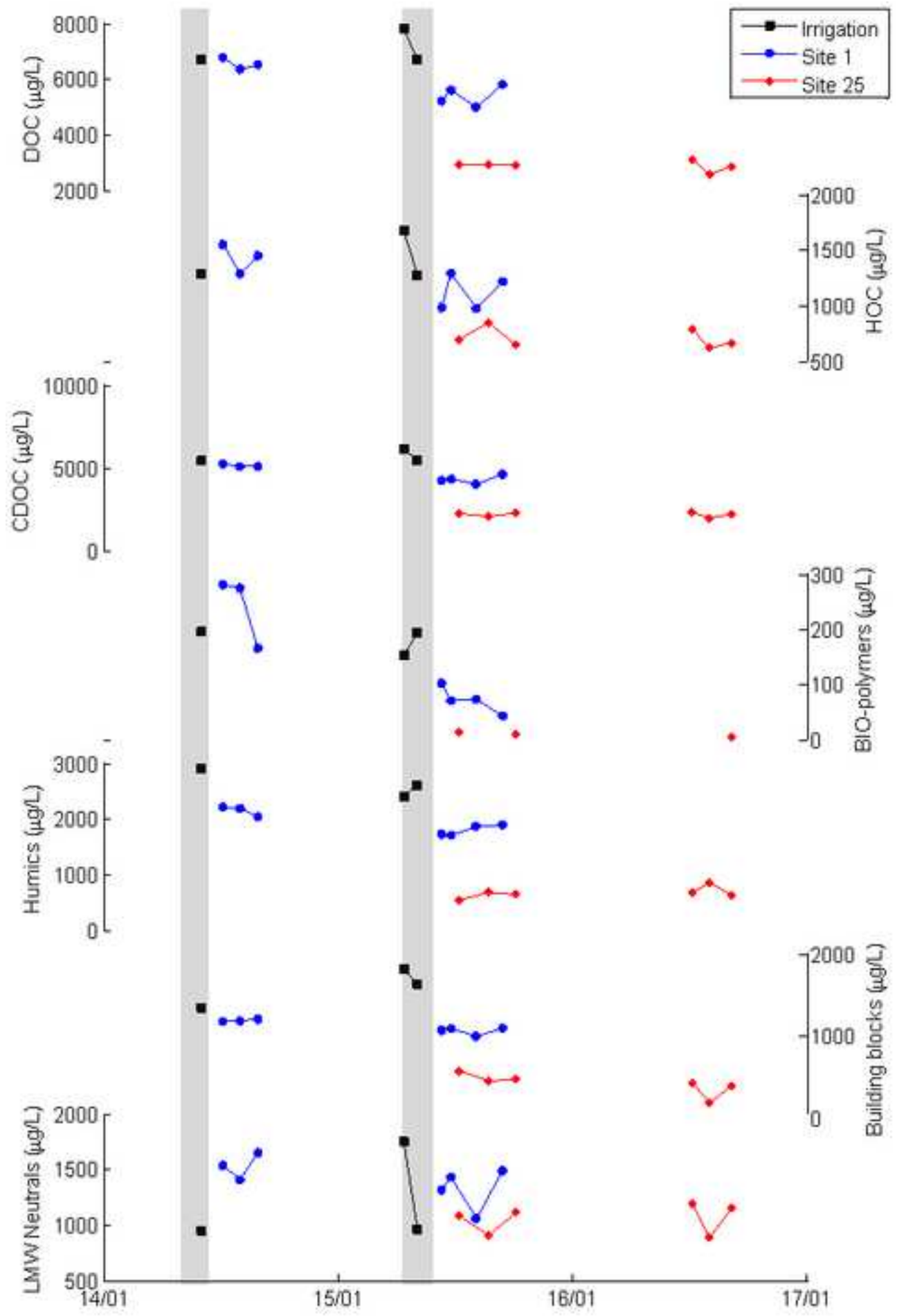


Figure5

[Click here to download high resolution image](#)

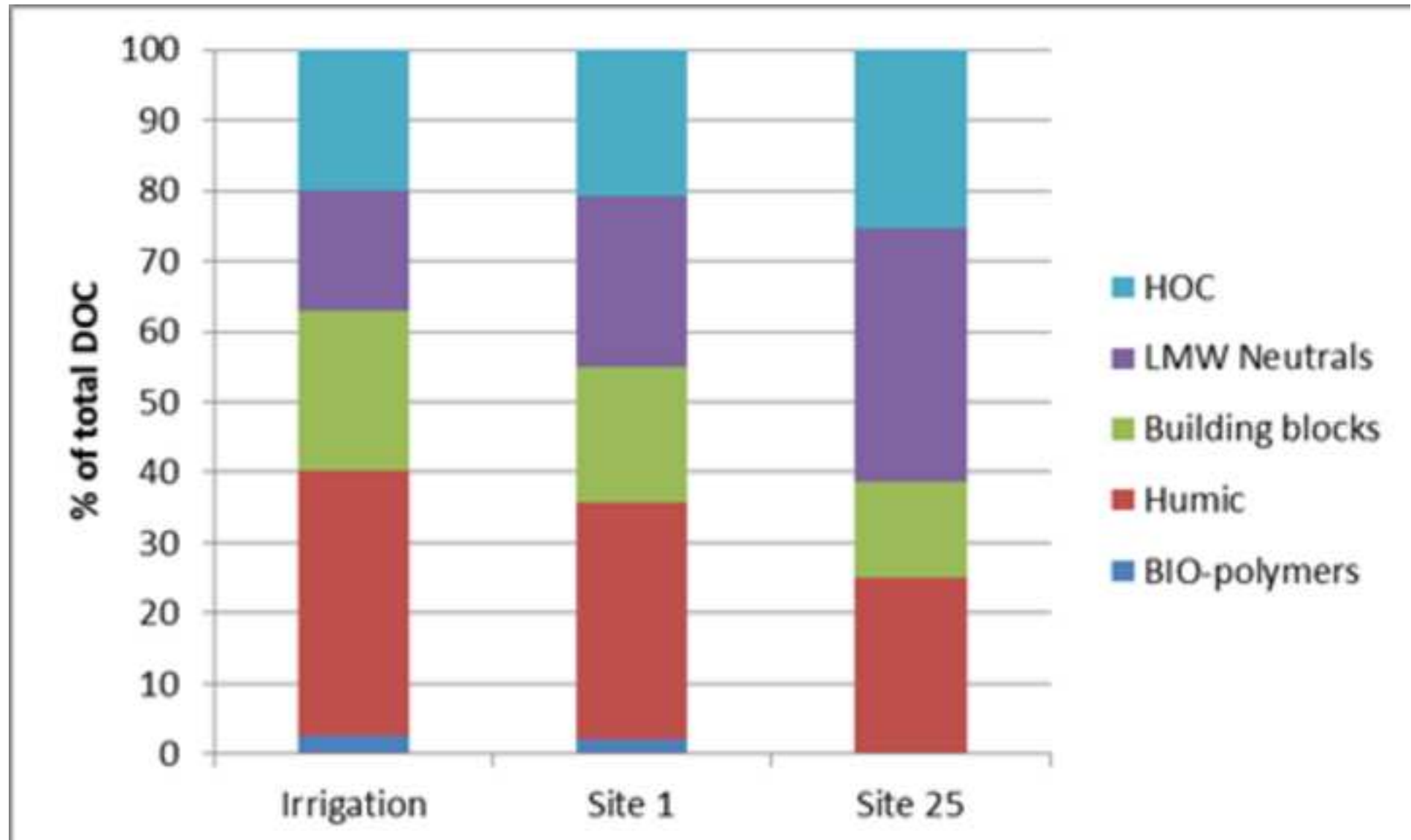


Figure6
[Click here to download high resolution image](#)

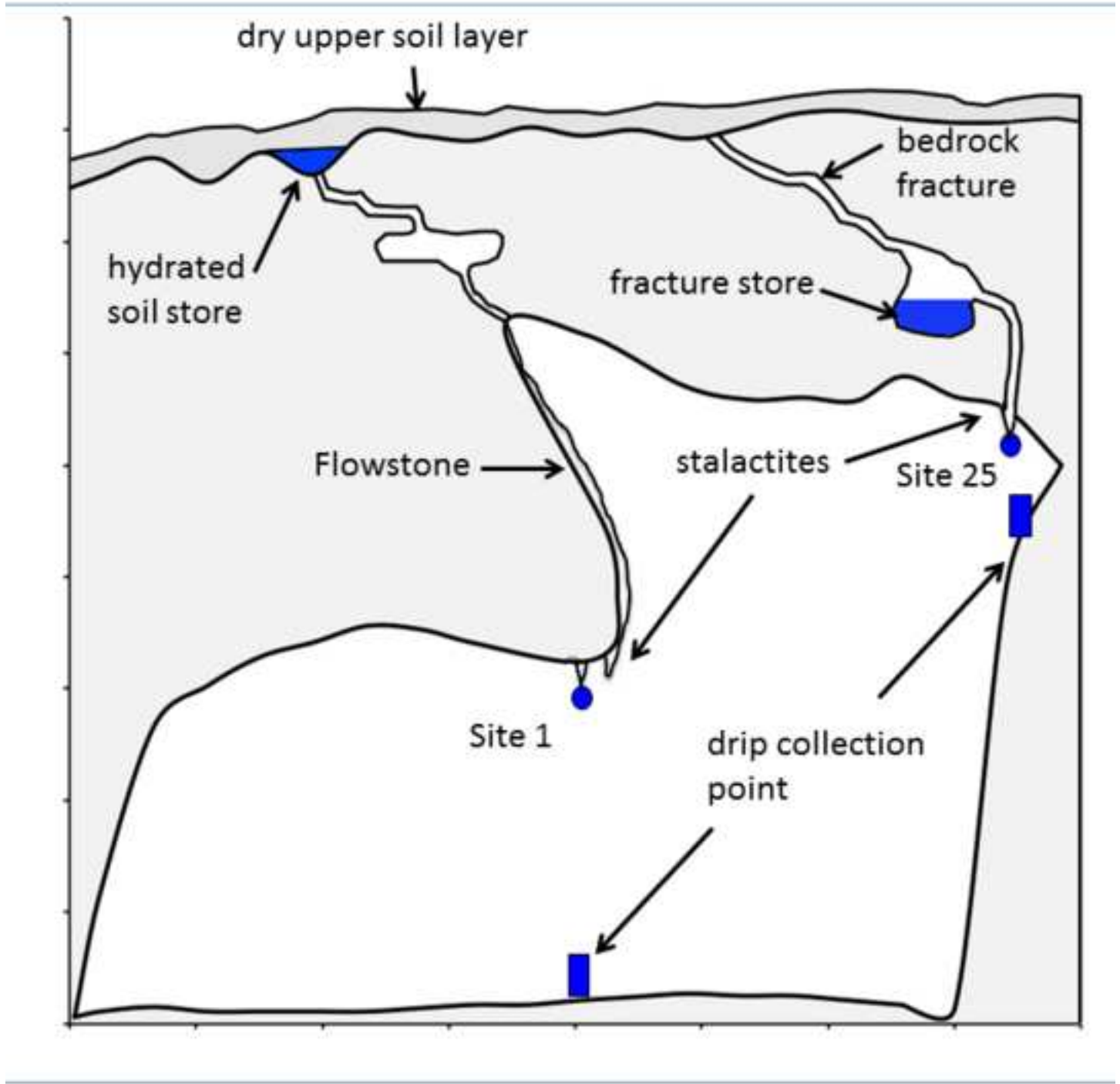


Figure7

[Click here to download high resolution image](#)

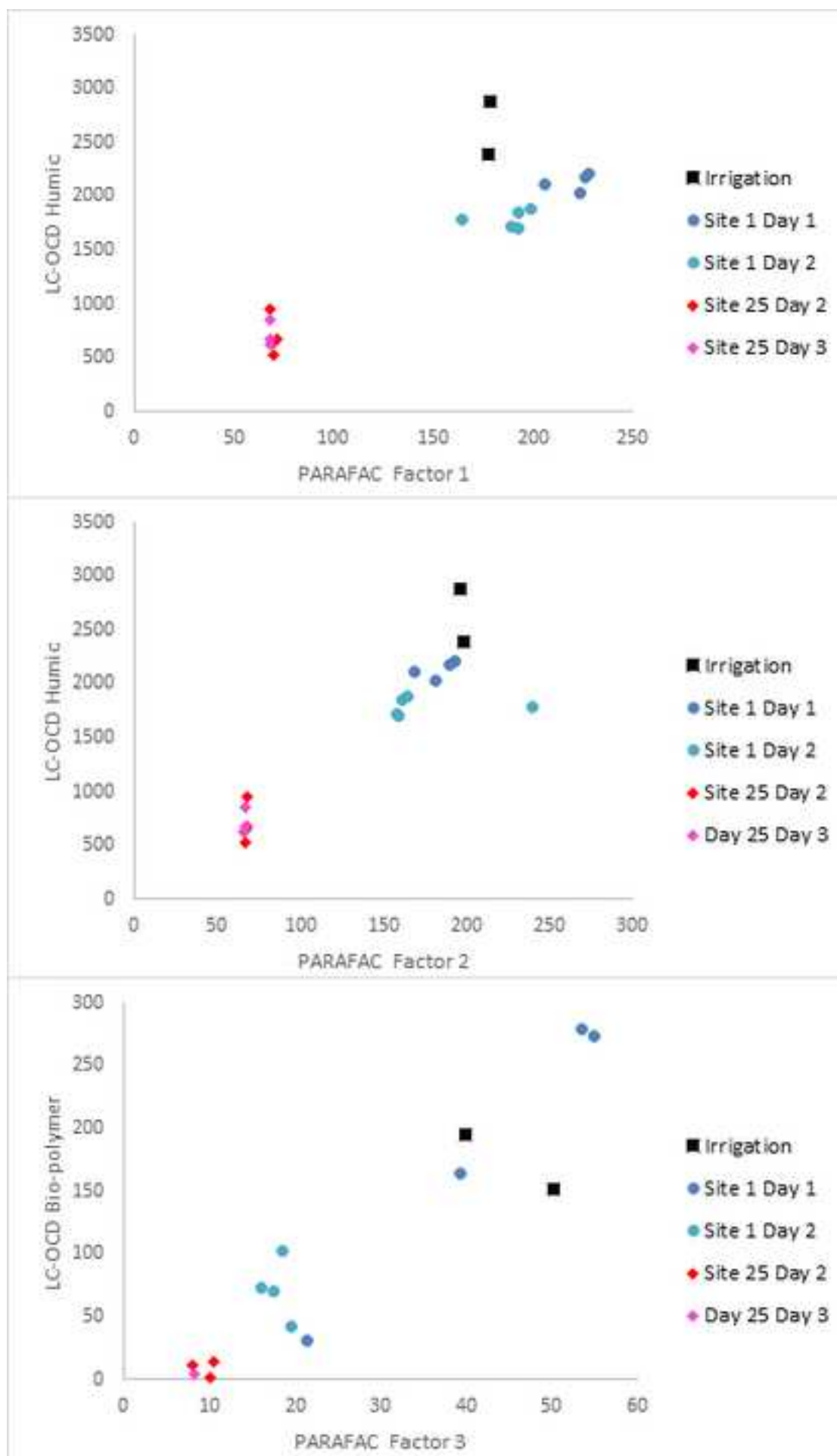


Figure8
[Click here to download high resolution image](#)

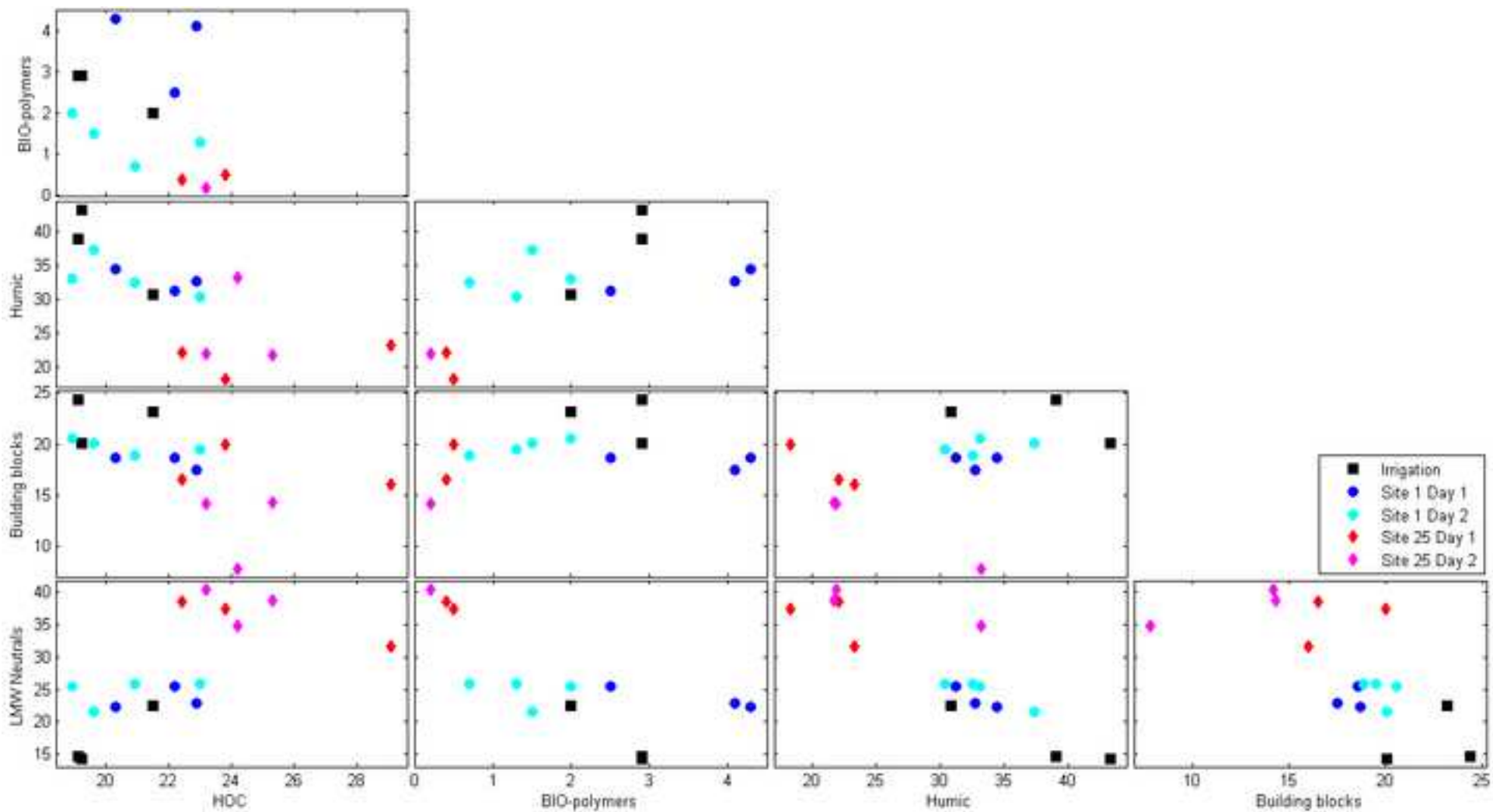
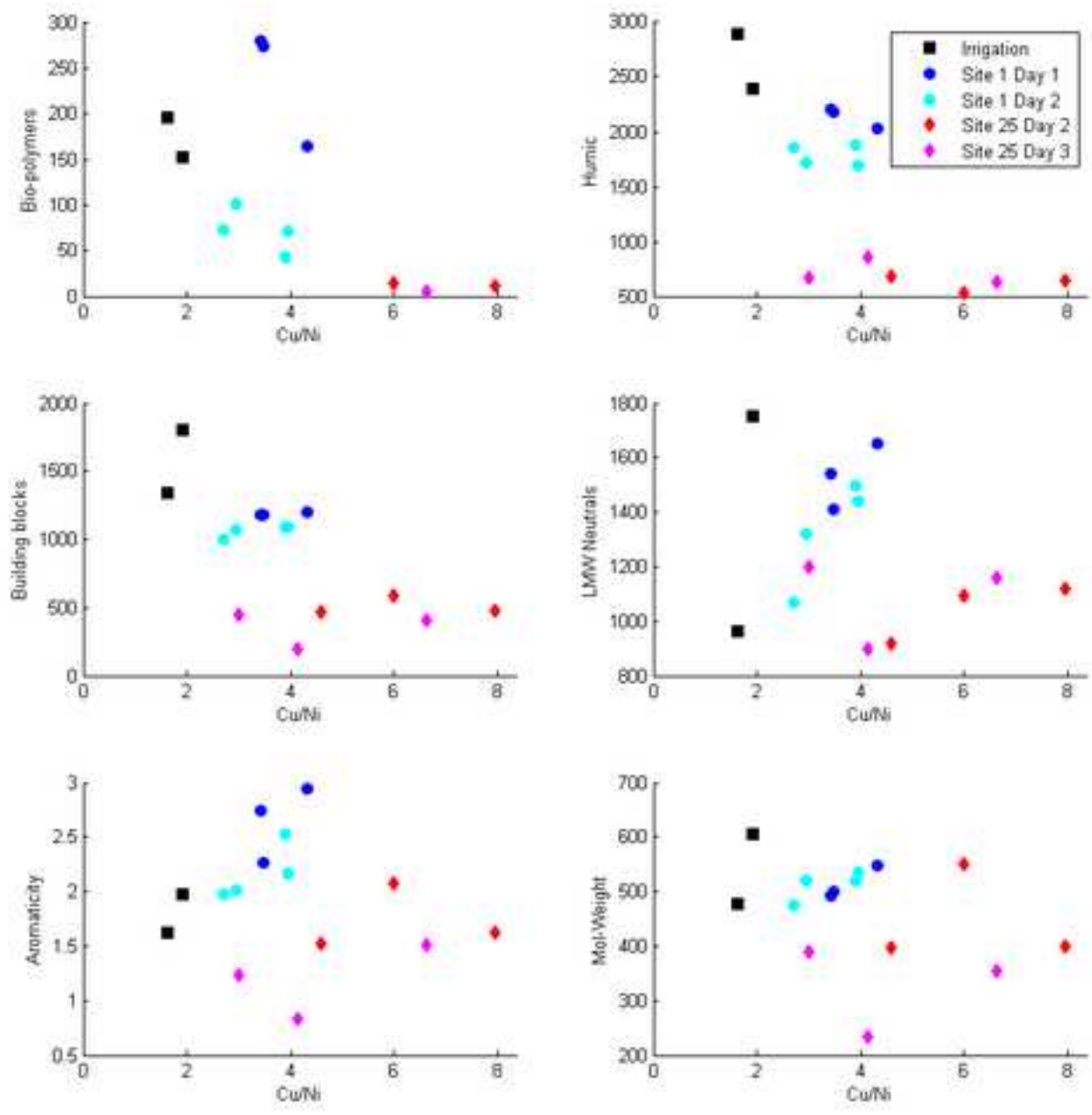


Figure9

[Click here to download high resolution image](#)



Supporting Data

[Click here to download Electronic Annex: Supporting data.docx](#)